HHS Public Access

Author manuscript

Biol Psychiatry. Author manuscript; available in PMC 2022 June 01.

Published in final edited form as:

Biol Psychiatry. 2021 June 01; 89(11): 1096–1105. doi:10.1016/j.biopsych.2020.12.022.

Ketamine rapidly enhances glutamate-evoked dendritic spinogenesis in medial prefrontal cortex through dopaminergic mechanisms

Mingzheng Wu, **Samuel Minkowicz**, **Vasin Dumrongprechachan**, **Pauline Hamilton**, **Yevgenia Kozorovitskiy***

Department of Neurobiology, Northwestern University, Evanston, IL 60208

Abstract

Background: Ketamine elicits rapid onset antidepressant effects in clinically depressed patients, through mechanisms hypothesized to involve the genesis of neocortical dendritic spines and synapses. Yet, the observed changes in dendritic spine morphology usually emerge well after ketamine clearance, raising questions about the link between rapid behavioral effects of ketamine and plasticity.

Methods: Here, we use 2-photon glutamate uncaging/imaging to focally induce spinogenesis in the medial prefrontal cortex (mPFC), directly interrogating baseline and ketamine-associated plasticity of deep layer pyramidal neurons in C57BL/6 mice. We combine pharmacological, genetic, optogenetic, and chemogenetic manipulations to interrogate dopaminergic mechanisms underlying ketamine-induced rapid enhancement in evoked plasticity and associated behavioral changes.

Results: We find that ketamine rapidly enhances glutamate-evoked spinogenesis in mPFC, with timing that matches the onset of its behavioral efficacy and precedes changes in dendritic spine density. Ketamine increases evoked cortical spinogenesis through Drd1 receptor activation that requires dopamine release, compensating blunted plasticity in a learned helplessness paradigm. The enhancement in evoked spinogenesis after Drd1 activation or ketamine treatment depends on postsynaptic Protein Kinase A (PKA) activity. Furthermore, ketamine's behavioral effects are blocked by chemogenetic inhibition of dopamine release and mimicked by activating presynaptic dopaminergic terminals, or postsynaptic $G\alpha_s$-coupled cascades in mPFC.

Conclusions: Our findings highlight dopaminergic mediation of rapid enhancement in activity-dependent dendritic spinogenesis and behavioral effects induced by ketamine.

*Corresponding author: Yevgenia.Kozorovitskiy@northwestern.edu.

The authors declare no biomedical financial interests or potential conflicts of interest. A part of this study, along with additional data, has been posted on bioRxiv: https://www.biorxiv.org/content/10.1101/2020.03.11.987818v2.full.

Keywords

Ketamine; dopamine; medial prefrontal cortex; dendritic spine; spinogenesis; 2-photon glutamate uncaging

INTRODUCTION

Ketamine and its S-enantiomer esketamine demonstrate rapid onset and lasting antidepressant effects in clinical studies (1,2); esketamine (Spravato) has been recently approved by the Food and Drug Administration for treatment-resistant depression (3). Ketamine acts primarily as an antagonist at the glutamatergic N-methyl-D-aspartate (NMDA) receptors (4-8), although several studies implicate mechanisms beyond direct NMDAR antagonism (9,10). Ketamine has been shown to ameliorate depressive-like behaviors in animal models of stress (11-15). Accumulating evidence implicates the enhancement of synaptic plasticity in ketamine's behavioral effects (6,8,13,14,16-19). Several prior studies demonstrate that *in vivo* administration of ketamine enhances dendritic spine density (16,20-23) and restores dendritic spine loss in the medial prefrontal cortex (mPFC) (19). Notably, increased dendritic spine density in mPFC pyramidal neurons usually emerges 12-24 hrs after a single subanesthetic dose of ketamine (16,19,20,23), yet clinical effects on behavior emerge within 2-4 hrs (1,2,24). Even if ketamine's effects on plasticity are linked to its behavioral efficacy, as has been suggested (16,19,21,23,25), this temporal mismatch could in principle result from a rapid enhancement of spinogenesis by ketamine, which over time leads to increased dendritic spine density. This possibility has not yet been directly examined.

Changes in hedonic, motivational, and aversive processing represent fundamental features of major depressive disorders (26-29). Reward, aversion, and motivational states are strongly tied to changes in the activity of midbrain dopaminergic (DA) neurons (30-35). In addition, dysregulation of DA systems has been demonstrated in clinically depressed patients (36,37) and in animal models of depression (38-41). The reversal of deficits in the DA system usually improves depressive-like behaviors (39,40,42). A recently published meta-analysis suggests that acute sub-anesthetic doses of ketamine increase DA levels in the prefrontal cortex (43), reported for both *in vivo* and *ex vivo* studies (44-48). Yet, little is known about the behavioral and neurobiological consequences of elevated cortical dopamine level induced by ketamine treatment. Outside the context of ketamine effects on the brain, several studies have elucidated DA modulation of intrinsic excitability and ion channel properties of mPFC pyramidal neurons (49-52). Whether DA signaling regulates structural plasticity of dendritic spines in mPFC and whether changes in DA tone account for ketamine-associated plasticity remains unknown.

Here, we rely on dual laser 2-photon glutamate uncaging and imaging to directly induce *de novo* dendritic spinogenesis on mPFC pyramidal neurons. The spatiotemporal control of this assay enables us to evaluate the capacity for spinogenesis independently from pre-existing dendritic spines. Combining this assay with pharmacological, genetic, and

behavioral manipulations allows us to functionally dissect the underlying mechanism of changes in the glutamate-evoked genesis of new dendritic spines.

METHODS AND MATERIALS

A detailed description of experimental procedures, including mouse strains and genotyping, stereotactic injections and optic fiber implants, behavior assays, local drug infusion, acute slice preparation, pharmacology, tissue processing and immunohistochemistry, and quantitative fluorescence *in situ* hybridization is provided in the Supplementary Information.

Mouse strains and genotyping.

Animals were handled according to protocols approved by the Northwestern University Animal Care and Use Committee. Weanling and young adult male and female mice (postnatal days 25-60) were used in this study. Approximately equal numbers of males and females were used for every experiment. All mice were group-housed, with standard feeding, light-dark cycle, and enrichment procedures; littermates were randomly assigned to conditions.

Behavior assays

Learned helplessness (LH).—P40-60 mice were used for behavioral assays with optogenetic and chemogenetic experiments. P25-40 mice were used for spinogenesis assays with behavioral manipulations. The learned helplessness procedure consisted of two induction sessions (1 session per day; 360 inescapable foot shocks per session; 0.3 mA, 3 sec; random 1-15 sec inter-shock intervals). Active/Passive Avoidance Shuttle Boxes from MazeEngineers (Boston, MA) were used for the experiment. To assess the degree of aversive learning, test sessions (30 escapable foot shocks per session; 0.3 mA, 10 sec; random 5-30 sec inter-shock intervals) were conducted before induction, 24 hrs after the last induction session, and following pharmacological or optogenetic manipulations. The testing was performed in a shuttle box (18 × 18 × 20 cm) equipped with a grid floor and a door separating the two compartments. No conditioned stimulus was delivered either before or after the shocks. Escapes were scored when the animal shuttled between compartments during the shock. Escape latency was measured as the time from the start of the shock to the escape. The shock automatically terminated when the animal shuttled to the other compartment. Failures were scored when the animal failed to escape before the shock end. The weaker LH paradigm (wLH) consisted of one induction session, and one test session with a larger number of brief escapable shocks (100 escapable foot shocks per session; 0.3 mA, 3 sec; random 5-15 sec intershock intervals). All behavioral assays were conducted during the active phase of the circadian cycle. Schematics involving mice were made using BioRender.

Two-photon imaging with two-photon glutamate uncaging

Dendritic imaging and uncaging of MNI-glutamate for spinogenesis induction were accomplished on a custom-built microscope combining two-photon laser-scanning microscopy (2PLSM) and two-photon laser photoactivation, as previously described (53-55). Two mode-locked Ti:Sapphire lasers (Mai Tai eHP and Mai Tai eHP DeepSee, Spectra-

Physics, Santa Clara, CA) were tuned to 910 and 725 nm for exciting EGFP and uncaging MNI-glutamate, respectively. The intensity of each laser was independently controlled by Pockels cells (Conoptics, Danbury, CT). A modified version of Scanimage software was used for data acquisition (56). For glutamate uncaging, 2.5 mM MNI-caged-L-glutamate (Tocris) was perfused into the slice chamber, and 725 nm light guided through a galvo scanhead was used to focally release the caging group. Secondary and tertiary dendritic branches were selected for dendritic imaging and spinogenesis induction. MNI-glutamate was uncaged near the dendrite (~0.5 μm) at 2 Hz using up to forty 2 ms-long pulses. Images were continually acquired during the induction protocol at 1 Hz, and uncaging was stopped if a spinehead was visible before 40 uncaging pulses were delivered. Analysis was carried out on raw image stacks and z projections. For display purposes only, a subset of the 2-photon micrographs was processed using Candle (57). A successful induction of new dendritic spine was scored when a protrusion from the dendrite in the uncaging location was observed. A newly generated dendritic spine had to satisfy the following criteria: *de novo* protrusion from the dendrite within 1 μm of the uncaging site; mean spine head fluorescence matching average fluorescence of spine heads on the parent dendrite; mean spine head fluorescence exceeding 20% of intensity in the parent dendrite. Changes in fluorescence intensity were profiled using line-scan analyses. For each animal, the probability of spinogenesis is represented as the fraction of successful induction trials out of all conducted trials within the individual.

Quantification of dendritic spine density

Sections of mPFC were either examined with a custom-built 2PLSM or a Leica SP5 confocal microscope (Leica Microsystems). Distal apical dendritic segments were selected for analysis. For each dendritic segment, dendritic spines protruding on both sides of the dendrite were marked using a 3D reconstruction system Neurolucida 360 (MBF Bioscience, Williston, VT). Six to eight z stacks (0.3 μm between each stack), at 0.07 μm lateral pixel size, were used for reconstruction. Dendritic spine density was averaged from 8-12 dendritic segments for each animal.

Statistical analyses

Group statistical analyses were done using GraphPad Prism 7 software (GraphPad, LaJolla, CA). For N sizes, the number of trials or cells recorded, as well as the number of animals are provided. All data are expressed as mean ± SEM, or individual plots. Probabilities are expressed as aggregate probabilities within individuals. For two-group comparisons, statistical significance was determined by two-tailed Student’s t-tests. For multiple group comparisons, one-way or two-way analysis of variance (ANOVA) tests were used for normally distributed data, followed by post hoc analyses. For non-normally distributed data, non-parametric tests for the appropriate group numbers were used. Pearson regression was used to detect the correlation between two groups of data. $p < 0.05$ was considered statistically significant.

RESULTS

Ketamine rapidly enhances glutamate-evoked spinogenesis in mPFC pyramidal neurons

Acute slices of mPFC were prepared from P25-40 mice of both sexes following neonatal transduction of sparse EGFP expression accomplished by a combination of AAV1.hSyn.Cre and AAV8.FLEX.EGFP. We imaged EGFP-labeled dendrites of layer 5 pyramidal neurons in mPFC using 2-photon laser scanning microscopy (2PLSM, 910 nm). A second laser was tuned to 725 nm to locally uncage MNI-glutamate near dendrites to probabilistically induce the formation of new dendritic spines (Figure 1A), as previously described for developing neurons in the striatum and superficial layers of sensory and motor cortex (53,55,58). Successful and unsuccessful induction trials of *de novo* spinogenesis were distinguished in z-stack projections through a dendritic segment before and after the brief induction protocol (< 30 sec) of up to 40 uncaging pulses (Figure 1B). In order to be classified as newly induced dendritic spines, the new membrane protrusions had to satisfy several criteria based on location and fluorescence intensity, relative to parent dendrite and pre-existing dendritic spines (methods and Supplementary Figure 1A-C).

We carried out evoked spinogenesis assays in different mice at several time points (2-72 hours) after a single subanesthetic dose of ketamine (10 mg/kg, i.p.). *In vivo* administration of ketamine in naive animals enhanced evoked *de novo* spinogenesis 2 and 4 hours after treatment (Figure 1C), temporally matching the emergence of ketamine's behavioral effects (4,5). This effect was transient, by 12 hours after ketamine was administered, the probability of spinogenesis decreased back to baseline levels. In addition, dendritic spine density was quantified at the same time points. In contrast to the rapid, transient changes in evoked spinogenesis, the increase in dendritic spine density was delayed until 12 hours after treatment (Figure 1C), consistent with prior reports (14,18-20). This temporal precedence of ketamine-associated potentiation of evoked spinogenesis suggests that changes in the potential for activity-dependent plasticity may contribute to slower, accumulating increases in spine density after ketamine treatment.

Rapid enhancement in evoked spinogenesis requires Drd1-PKA signaling

Given the hypothesized links between ketamine and the DA system, we sought to determine whether ketamine's effect on evoked plasticity is mediated by the activation of DA receptors. First, we verified the expression of Drd1a receptors in EGFP-expressing neurons. Consistent with prior reports (59,60), the majority of pyramidal neurons in the deep layers of mPFC express *Drd1a* mRNA (Figure 1D, Supplementary Figure 2A, B). We compared glutamate-evoked spinogenesis after administering ketamine alone, or in conjunction with a Drd1 receptor antagonist SKF 83566 (10 mg/kg i.p., 2 hours prior to *ex vivo* experiments). We found that antagonizing Drd1 receptors blocked ketamine's potentiation of evoked spinogenesis, while the antagonist treatment alone had no effect relative to baseline (Figure 1D). Thus, while the activation of Drd1 receptors in this neuronal population is not required for baseline glutamate-evoked plasticity, it appears to be necessary for ketamine's enhancement of evoked spinogenesis.

Next, in order to suppress mPFC DA release without broadly altering Drd1 activation and locomotor behavior (61), we used chemogenetic inhibition of VTA DA neurons; the major source of DA in mPFC. Inhibiting hM4Di$^+$ VTA DA neurons with CNO (3 mg/kg, i.p.) while administering ketamine treatment blocked ketamine's spinogenesis-enhancing effects (Figure 1E). Yet, as for the pharmacological Drd1 receptor blockade *in vivo*, we observed no effects of CNO treatment on evoked spinogenesis in the absence of ketamine. These observations are consistent with a model where the genesis of new dendritic spines and synapses mechanistically depends on glutamate, but the enhancement of this plasticity requires the activation of PKA via $G\alpha_s$-coupled receptors (55). In addition to blocking ketamine-mediated enhancement of evoked spinogenesis, transient inhibition of VTA DA neuron activity (a single CNO dose + ketamine) also abolished the delayed increase of spine density 24 hours after ketamine (Figure 1F). These data show that in the absence of behavioral manipulations, Drd1 activation and VTA DA activity regulate changes in spinogenesis and dendritic spine density, mediating the effects of ketamine on plasticity in mPFC.

The next series of experiments test whether the capacity for spinogenesis is altered in animal models of stress, where ketamine ameliorates behavior. We exposed mice to subacute uncontrollable stress by administering foot shocks over 2 days, using an adapted model of learned helplessness (LH, 3 sec inescapable, 360 shocks each day, Figure 2A). Following repeated exposure to inescapable foot shocks, LH behavior manifests in increased failures to escape from readily avoidable shocks (10 sec escapable, 30 trials total), consistent with prior reports (38,62). A single dose of ketamine 4 hours prior to the test (10 mg/kg, b.w., i.p.) is sufficient to rescue escape behavior in this paradigm (Figure 2B). We next tested glutamate-evoked spinogenesis in the baseline, after stress exposure (LH), and following ketamine treatment (LH + KET). The probability of glutamate evoked spinogenesis decreased relative to baseline in LH mice, while ketamine treatment restored the baseline potential for plasticity (Figure 2C). We found that 2 days of stressful experience is sufficient to decrease the potential of spinogenesis in mPFC pyramidal neurons, in contrast to changes in dendritic spine density that normally manifest after chronic stress (16,63,64). No significant sex difference was observed across conditions, despite a trend towards higher evoked spinogenesis in females in the baseline condition (Supplementary Figure 3A-B). To correlate individual behavioral outcomes with evoked plasticity, we performed *de novo* spinogenesis assays in animals trained with a modified, weaker LH paradigm (wLH), with or without subsequent ketamine treatment. In the wLH paradigm, we used a larger number of brief (3 sec) escapable foot shocks to evaluate the escape behavior, following a single day of LH induction with inescapable shocks (Supplementary Figure 3C). We found that the probability of evoked spinogenesis negatively correlates with the percentages of failures to escape in both conditions (wLH +/− ketamine) (Supplementary Figure 3D). This result suggests that mPFC plasticity is linked to behavioral profiles of individual animals after LH and ketamine treatment.

We then tested the contribution of Drd1 receptors to ketamine related plasticity changes. To specifically manipulate Drd1 receptor expression in mPFC without affecting the global DA system, we conditionally knocked out Drd1 receptors by co-expressing Cre recombinase and Cre-dependent EGFP in Drd1-floxed mice (Figure 2D). We validated the conditional knock-

out by verifying the expression of *Drd1a* mRNA in EGFP-expressing neurons (Figure 2D). Sparse genetic depletion of Drd1 receptor in mPFC pyramidal neurons abolished ketamine's effect on spinogenesis in LH animals, without changing the probability of spinogenesis for mice in the baseline or LH conditions (Figure 2E).

Next, we addressed the downstream signaling mechanism for DA enhancement of glutamate-evoked spinogenesis. Drd1 receptor activation is known to regulate glutamatergic synapse and dendritic spine formation in the developing striatum (55,65).Yet, mPFC Drd1 receptor expression levels in single neurons are considerably lower than in the striatum (mPFC Layer 5 pyramidal neurons: ~4/100,000 transcripts; striatum: ~110/100,000; data from DropViz (66)). We found that bath application of Drd1 agonist SKF 81297 (1 μM) promotes glutamate-evoked spinogenesis in mPFC pyramidal neurons (Figure 3A, B). This effect requires Drd1a signaling, since Drd1a cKO abolished the enhancement of spinogenesis. Suppression of PKA activity by either bath application of H-89 (10 μM) or over-expression of endogenous PKA inhibitor (PKIα) in mPFC pyramidal neurons blocked changes in spinogenesis induced by SKF 81297 (Figure 3B, C). In addition, *in vivo* pre-treatment with ketamine (10 mg/kg, i.p.) occluded the enhancement of spinogenesis by SKF 81297 (Figure 3D), supporting the argument that ketamine's effect on structural plasticity is mediated by Drd1 receptor. Furthermore, the plasticity-promoting effect of ketamine was blocked by over-expression of PKIα (Figure 3E). Several established targets of PKA, involved in cytoskeletal remodeling, could contribute to Drd1-dependent effects of ketamine on structural plasticity (67) (Figure 3F). Altogether, our results reveal that ketamine's rapid modulation of structural plasticity in mPFC pyramidal neurons requires the Drd1a-PKA signaling cascade.

Bidirectional manipulation of mPFC DA release controls behavioral effects of ketamine

To connect the mechanisms of ketamine-associated plasticity and its behavioral effects, we examined the role of cortical DA signaling in escape behavior after LH. To induce local dopamine release in mPFC, we optogenetically activated DA terminals in mPFC in animals with ChR2 expression restricted to VTA DA neurons. DAT^{icre} neonates were transduced with AAV1.EF1α.DIO.hChR2(H134R).eYFP, or a control fluorophore, and implanted with optical fibers 4-6 weeks after transduction (Figure 4A, B). After LH induction, animals received a series of burst optogenetic stimuli at 20 Hz every 10 sec (10 pulses, 20 ms width, 500 ms duration) during the test session consisting of 30 avoidable foot shocks (Figure 4C). The stimulation bursts were not timed relative to shocks and took place on either side of the shuttle box, decreasing the likelihood of forming conditioned place preference or aversion. Optogenetic activation of DA axon terminals in mPFC significantly decreased the percentage of failures after LH, as well as latencies to escape (Figure 4D). Optogenetic stimulation did not alter locomotion behavior in either the open field or the shuttle box, suggesting the high escape tendency is not caused by hyperlocomotion (Figure 4E). Thus, enhancing DA release in mPFC is sufficient to rescue escapes after LH.

While we find that optogenetically driven increase in mPFC DA tone mimics behavioral effects of ketamine, whether these effects require local DA release in mPFC remains unclear. To achieve local inhibition of DA release, we infused CNO into the mPFC

of mice expressing hM4Di in VTA DA neurons and their terminals in mPFC to reduce axonal release of dopamine (68-70). DAT^{iCre} neonates were transduced with AAV1.CBA.DIO.hM4Di.mCherry in the VTA, and cannulae were implanted bilaterally over mPFC in order to locally deliver 1 mM CNO (1 μl for each side) (Figure 4F and Supplementary Figure 4A). A high density of hM4Di.mCherry expression in mPFC terminals was observed in immunoenhanced fixed tissue sections (Figure 4G). Local infusion of CNO in mPFC along with ketamine treatment blocked the behavioral effect of ketamine (10 mg/kg, i.p.) in the LH paradigm, while ketamine alone was sufficient to rescue escape behavior (Figure 4H and Supplementary Figure 4B). To determine whether mPFC DA function is required to maintain the effect of ketamine on behavior, we chemogenetically inhibited DA release 24 hours after ketamine treatment (Supplementary Figure 4C). This delayed manipulation had no significant effect on escape behaviors. Together, these results suggest that disruption of DA signaling is important for ketamine effects during an initial narrow time window following ketamine administration.

The activation of Drd1 receptors initiates $G\alpha_s$ mediated PKA signaling cascades, which enhance spinogenesis, synaptic transmission, and neuronal activity (54,55,59,71). We therefore tested whether selective activation of $G\alpha_s$ signaling in mPFC Drd1 expressing neurons could rescue escape behavior after aversive learning. We relied on the $G\alpha_s$-coupled rM3D DREADD, expressing AAV1.CBA.DIO.rM3Ds.mCherry in Drd1-Cre-FK150 mice (Figure 4I). The expression of rM3Ds alone did not change baseline escape and failure rates, or the magnitude of aversive learning. After LH induction, a single i.p. dose of CNO was sufficient to rescue escape behavior 4 hours after treatment, lasting at least 24 hours (Figure 4I). Activating $G\alpha_s$ signaling in Drd1a expressing neurons *in vivo* significantly increased phosphorylation of CREB, which is typically induced by $G\alpha_s$-coupled cascades (Figure 4J). In addition to our results, a recently published study showed that optogenetic activation of $Drd1^+$ mPFC neurons decreases immobility time in the forced swim test, suggesting that these Drd1-expressing neurons may broadly regulate aversive or active coping responses (72). Altogether, our data demonstrate that mPFC DA signaling mediates both the rapid plasticity-promoting actions and behavioral effects of ketamine.

DISCUSSION

Glutamate-evoked interrogation of plasticity on genetically targeted neurons offers unique strengths as a structural plasticity readout. Besides dissociating *de novo* genesis and elimination of dendritic spines and synapses, this assay facilitates pharmacological and genetic mechanism dissection and is compatible with behavioral manipulations. Our observations demonstrate a temporal precedence of spinogenesis increase relative to changes in dendritic spine density, suggesting that the changes in spine density *in vivo* can be due to a prior, accumulating change in glutamatergic activity-dependent spinogenesis. Recent work demonstrates that newly formed dendritic spines are required to maintain the behavioral effect of ketamine after chronic corticosterone administration (19), establishing a causal link between the increase in new spine formation and ketamine's behavioral effects. Here, we have defined the mechanisms underlying rapid changes in spinogenesis that are required for these causal effects.

The current study explains several intriguing temporal observations about ketamine actions and reconciles previously reported temporal mismatches. First, rapid anti-depressant effects of ketamine usually begin 2-4 hours after a single dose of treatment (2,4,24,73), while changes in dendritic spine morphology in mPFC are primarily observed 8-16 hours later (14,16,19,23). Our results reveal that the enhancement of glutamate-induced spinogenesis occurs rapidly (2-4 hours) after ketamine treatment, corresponding to its rapid-onset behavioral effects. Second, the half-life of ketamine is estimated at 1-3 hours in humans (~1.5 hours in rodents), with a relatively short clearance time (~8-12 hours) (74,75). These short clearance times stand in contrast to the lasting behavioral effects of ketamine in both humans and rodents (> 24 hours) (1,2,24). Given this temporal difference, one intriguing possibility is that the timing of the clinical anti-depressant effects of ketamine in MDD patients (~1 week following a single dose) derives from a lasting change in DA-dependent structural plasticity caused by ketamine. Exactly how new dendritic spines stabilize and contribute to behavior after ketamine treatment may further reveal how ketamine's effects last days beyond its bioavailability. Since our experiments were carried out in young animals and neural plasticity dynamics are known to change across age (76-78), the efficacy of ketamine treatment could vary in clinical populations as a function of age, even if mechanisms of action are conserved. Since DA tone in mPFC changes through the lifespan (79-82), the variance in ketamine's antidepressant efficacy (*e.g.* low efficacy and more transient effects for geriatric depression (83)) may be partially explained by the age-related alterations in cortical DA tone.

This work ties into a growing body of literature explicitly and implicitly linking ketamine, behavior, and plasticity. A recent study concluded that Drd1-positive neurons in mPFC regulate depressive-like behavior (72), and our study investigated the underlying neuromodulatory and plasticity mechanisms consistent with this discovery. Together, the two studies support the idea that ketamine controls mPFC plasticity and behaviors through cortical modulation by DA. Another recent paper demonstrates that newly formed dendritic spines are required to maintain the behavioral effect of ketamine after chronic corticosterone administration (19), establishing a causal link between the increase in new spine formation and ketamine's behavioral effects. These findings, together with our observations of correlated spinogenesis and escape behavior after LH, highlight the importance of new dendritic spine formation for behavioral regulation. Future experiments are required to fully understand the impact of individual variability in plasticity and neuromodulatory signaling on the anti-depressant effects of ketamine.

Our observations that DA signaling mediates of dendritic spine plasticity in mPFC after ketamine injection, may reflect broadly conserved mechanisms in the brain, where DA controls activity-induced plasticity of dendritic spines and excitatory synapse formation. Prior data demonstrate that, during development, DA regulates the formation of dendritic spines and excitatory synapses in striatal direct pathway spiny projection neurons expressing Drd1 receptors (55,65). The activation of Drd1 receptors stimulates $G\alpha_s$ signaling cascades, increasing cAMP production and PKA activity. Analogously, DA promotes glutamate-evoked spinogenesis on mPFC pyramidal neurons through Drd1 receptor activation and changes in PKA activity. Given that actin dynamics are important for dendritic spine formation and shape regulation (84), the mechanistic link between Drd1-PKA signaling

and dendritic spine formation likely involves cytoskeleton remodeling proteins. Indeed, PKA modulates the activity of small GTPases (*e.g.*, Rap1, Rac1, Cdc42, among others) known to regulate dendritic spines (67) through guanine nucleotide exchange factors (GEFs) and GTPase-activating proteins (GAPs) (85,86). Specific molecular effectors responsible for ketamine-induced changes in synaptic and dendritic spine plasticity remain to be elucidated and may provide new clinical targets.

Supplementary Material

Refer to Web version on PubMed Central for supplementary material.

ACKNOWLEDGEMENTS AND DISCLOSURES

The authors are grateful to Lindsey Butler for mouse colony management, Northwestern Biological Imaging Facility and Dr. Tiffany Schmidt for confocal microscope access. This work was supported by the Rita Allen Foundation Scholar Award, NINDS R01NS107539, Searle Scholar Award, the Beckman Young Investigator Award, William and Bernice E. Bumpus Young Innovator Award, NARSAD Young Investigator, and P&S Fund Grant (all Y.K.). M.W was supported as an affiliate fellow of the NIH T32 AG20506, S.M. is a fellow of the National Science Foundation Graduate Research Fellowship DGE-1842165, and V.D. is a predoctoral fellow of the American Heart Association (19PRE34380056).

REFERENCES

1. Daly EJ, Singh JB, Fedgchin M, Cooper K, Lim P, Shelton RC, et al. (2018): Efficacy and safety of intranasal esketamine adjunctive to oral antidepressant therapy in treatment-resistant depression: A randomized clinical trial. JAMA Psychiatry 75: 139–148. [PubMed: 29282469]
2. Berman RM, Cappiello A, Anand A, Oren DA, Heninger GR, Charney DS, Krystal JH (2000): Antidepressant effects of ketamine in depressed patients. Biol Psychiatry 47: 351–354. [PubMed: 10686270]
3. Kim J, Farchione T, Potter A, Chen Q, Temple R (2019): Esketamine for Treatment-Resistant Depression — First FDA-Approved Antidepressant in a New Class. N Engl J Med 381: 1–4. [PubMed: 31116916]
4. Duman RS (2018): Ketamine and rapid-acting antidepressants: a new era in the battle against depression and suicide. F1000Research 7: 659.
5. Zanos P, Gould TD (2018): Mechanisms of ketamine action as an antidepressant. Mol Psychiatry 23: 801–811. [PubMed: 29532791]
6. Miller OH, Yang L, Wang C-C, Hargroder EA, Zhang Y, Delpire E, Hall BJ (2014): GluN2B-containing NMDA receptors regulate depression-like behavior and are critical for the rapid antidepressant actions of ketamine. Elife 3: e03581. [PubMed: 25340958]
7. Abdallah CG, Sanacora G, Duman RS, Krystal JH (2015): Ketamine and Rapid-Acting Antidepressants: A Window into a New Neurobiology for Mood Disorder Therapeutics. Annu Rev Med 66: 509–523. [PubMed: 25341010]
8. Holmes SE, Scheinost D, Finnema SJ, Naganawa M, Davis MT, DellaGioia N, et al. (2019): Lower synaptic density is associated with depression severity and network alterations. Nat Commun 10: 1529. [PubMed: 30948709]
9. Zanos P, Moaddel R, Morris PJ, Georgiou P, Fischell J, Elmer GI, et al. (2016): NMDAR inhibition-independent antidepressant actions of ketamine metabolites. Nature 533: 481–486. [PubMed: 27144355]
10. Wray NH, Schappi JM, Singh H, Senese NB, Rasenick MM (2019): NMDAR-independent, cAMP-dependent antidepressant actions of ketamine. Mol Psychiatry 24: 1833–1843. [PubMed: 29895894]
11. Harmer CJ, Duman RS, Cowen PJ (2017): How do antidepressants work? New perspectives for refining future treatment approaches. The Lancet Psychiatry 4: 409–418. [PubMed: 28153641]

12. Fuchikami M, Thomas A, Liu R, Wohleb ES, Land BB, DiLeone RJ, et al. (2015): Optogenetic stimulation of infralimbic PFC reproduces ketamine's rapid and sustained antidepressant actions. Proc Natl Acad Sci 112: 8106–8111. [PubMed: 26056286]
13. Duman RS, Aghajanian GK (2012): Synaptic dysfunction in depression: potential therapeutic targets. Science 338: 68–72. [PubMed: 23042884]
14. Duman RS, Aghajanian GK, Sanacora G, Krystal JH (2016): Synaptic plasticity and depression: New insights from stress and rapid-acting antidepressants. Nat Med 22: 238–249. [PubMed: 26937618]
15. Krishnan V, Nestler EJ (2011): Animal models of depression: molecular perspectives. Curr Top Behav Neurosci 7: 121–47. [PubMed: 21225412]
16. Li N, Lee B, Liu R-J, Banasr M, Dwyer JM, Iwata M, et al. (2010): mTOR-Dependent Synapse Formation Underlies the Rapid Antidepressant Effects of NMDA Antagonists. Science 329: 959–964. [PubMed: 20724638]
17. Popoli M, Yan Z, McEwen BS, Sanacora G (2012): The stressed synapse: The impact of stress and glucocorticoids on glutamate transmission. Nat Rev Neurosci 13: 22–37.
18. Gerhard DM, Wohleb ES, Duman RS (2016): Emerging treatment mechanisms for depression: focus on glutamate and synaptic plasticity. Drug Discov Today 21: 454–464. [PubMed: 26854424]
19. Moda-Sava RN, Murdock MH, Parekh PK, Fetcho RN, Huang BS, Huynh TN, et al. (2019): Sustained rescue of prefrontal circuit dysfunction by antidepressant-induced spine formation. Science 364: eaat8078. [PubMed: 30975859]
20. Phoumthipphavong V, Barthas F, Hassett S, Kwan AC (2016): Longitudinal effects of ketamine on dendritic architecture in vivo in the mouse medial frontal cortex. eNeuro 3: 91–95.
21. Sarkar A, Kabbaj M (2016): Sex Differences in Effects of Ketamine on Behavior, Spine Density, and Synaptic Proteins in Socially Isolated Rats. Biol Psychiatry 80: 448–456. [PubMed: 26957131]
22. Ng LHL, Huang Y, Han L, Chang RC-C, Chan YS, Lai CSW (2018): Ketamine and selective activation of parvalbumin interneurons inhibit stress-induced dendritic spine elimination. Transl Psychiatry 8: 272. [PubMed: 30531859]
23. Liu RJ, Fuchikami M, Dwyer JM, Lepack AE, Duman RS, Aghajanian GK (2013): GSK-3 inhibition potentiates the synaptogenic and antidepressant-like effects of subthreshold doses of ketamine. Neuropsychopharmacology 38: 2268–2277. [PubMed: 23680942]
24. Krystal JH, Sanacora G, Duman RS (2013): Rapid-Acting Glutamatergic Antidepressants: The Path to Ketamine and Beyond. Biol Psychiatry 73: 1133–1141. [PubMed: 23726151]
25. Krystal JH, Abdallah CG, Sanacora G, Charney DS, Duman RS (2019): Ketamine: A Paradigm Shift for Depression Research and Treatment. Neuron 101: 774–778. [PubMed: 30844397]
26. Proulx CD, Hikosaka O, Malinow R (2014): Reward processing by the lateral habenula in normal and depressive behaviors. Nat Neurosci 17: 1146–1152. [PubMed: 25157511]
27. Abler B, Erk S, Herwig U, Walter H (2007): Anticipation of aversive stimuli activates extended amygdala in unipolar depression. J Psychiatr Res 41: 511–522. [PubMed: 17010993]
28. Heldt SA, Stanek L, Chhatwal JP, Ressler KJ (2007): Hippocampus-specific deletion of BDNF in adult mice impairs spatial memory and extinction of aversive memories. Mol Psychiatry 12: 656–670. [PubMed: 17264839]
29. Luking KR, Pagliaccio D, Luby JL, Barch DM (2016, 6 1): Reward Processing and Risk for Depression Across Development. Trends in Cognitive Sciences, vol. 20. Elsevier Ltd, pp 456–468. [PubMed: 27131776]
30. Morales M, Margolis EB (2017): Ventral tegmental area: Cellular heterogeneity, connectivity and behaviour. Nat Rev Neurosci 18: 73–85. [PubMed: 28053327]
31. Berridge KC, Kringelbach ML (2015): Pleasure Systems in the Brain. Neuron 86: 646–664. [PubMed: 25950633]
32. Bromberg-Martin ES, Matsumoto M, Hikosaka O (2010): Dopamine in Motivational Control: Rewarding, Aversive, and Alerting. Neuron 68: 815–834. [PubMed: 21144997]
33. de Jong JW, Afjei SA, Pollak Dorocic I, Peck JR, Liu C, Kim CK, et al. (2019): A Neural Circuit Mechanism for Encoding Aversive Stimuli in the Mesolimbic Dopamine System. Neuron 101: 133–151.e7. [PubMed: 30503173]

34. Lammel S, Lim BK, Malenka RC (2014, 1): Reward and aversion in a heterogeneous midbrain dopamine system. Neuropharmacology, vol. 76. NIH Public Access, pp 351–359. [PubMed: 23578393]
35. Vander Weele CM, Siciliano CA, Matthews GA, Namburi P, Izadmehr EM, Espinel IC, et al. (2018): Dopamine enhances signal-to-noise ratio in cortical-brainstem encoding of aversive stimuli. Nature 563: 397–401. [PubMed: 30405240]
36. Dunlop BW, Nemeroff CB (2007, 3 1): The role of dopamine in the pathophysiology of depression. Archives of General Psychiatry, vol. 64. American Medical Association, pp 327–337. [PubMed: 17339521]
37. Dailly E, Chenu F, Renard CE, Bourin M (2004, 12 1): Dopamine, depression and antidepressants. Fundamental and Clinical Pharmacology, vol. 18. John Wiley & Sons, Ltd, pp 601–607. [PubMed: 15548230]
38. Belujon P, Grace AA (2014): Restoring mood balance in depression: Ketamine reverses deficit in dopamine-dependent synaptic plasticity. Biol Psychiatry 76: 927–936. [PubMed: 24931705]
39. Chaudhury D, Walsh JJ, Friedman AK, Juarez B, Ku SM, Koo JW, et al. (2013): Rapid regulation of depression-related behaviours by control of midbrain dopamine neurons. Nature 493: 532–536. [PubMed: 23235832]
40. Tye KM, Mirzabekov JJ, Warden MR, Ferenczi EA, Tsai H-C, Finkelstein J, et al. (2012): Dopamine neurons modulate neural encoding and expression of depression-related behaviour. Nature 493: 537–541. [PubMed: 23235822]
41. Belujon P, Grace AA (2017): Dopamine System Dysregulation in Major Depressive Disorders. Int J Neuropsychopharmacol 20: 1036–1046. [PubMed: 29106542]
42. Friedman AK, Walsh JJ, Juarez B, Ku SM, Chaudhury D, Wang J, et al. (2014): Enhancing Depression Mechanisms in Midbrain Dopamine Neurons Achieves Homeostatic Resilience. Science 344: 313–319. [PubMed: 24744379]
43. Kokkinou M, Ashok AH, Howes OD (2018): The effects of ketamine on dopaminergic function: Meta-Analysis and review of the implications for neuropsychiatric disorders. Mol Psychiatry 23: 59–69. [PubMed: 28972576]
44. Moghaddam B, Adams B, Verma A, Daly D (1997): Activation of glutamatergic neurotransmission by ketamine: A novel step in the pathway from NMDA receptor blockade to dopaminergic and cognitive disruptions associated with the prefrontal cortex. J Neurosci 17: 2921–2927. [PubMed: 9092613]
45. Verma A, Moghaddam B (1996): NMDA receptor antagonists impair prefrontal cortex function as assessed via spatial delayed alternation performance in rats: Modulation by dopamine. J Neurosci 16: 373–379. [PubMed: 8613804]
46. Chatterjee M, Verma R, Ganguly S, Palit G (2012): Neurochemical and molecular characterization of ketamine-induced experimental psychosis model in mice. Neuropharmacology 63: 1161–1171. [PubMed: 22683513]
47. Lindefors N, Barati S, O'Connor WT (1997): Differential effects of single and repeated ketamine administration on dopamine, serotonin and GABA transmission in rat medial prefrontal cortex. Brain Res 759: 205–212. [PubMed: 9221938]
48. Lorrain D, Baccei C, Bristow L, Anderson J, Varney M (2003): Effects of ketamine and n-methyl-d-aspartate on glutamate and dopamine release in the rat prefrontal cortex: modulation by a group II selective metabotropic glutamate receptor agonist LY379268. Neuroscience 117: 697–706. [PubMed: 12617973]
49. Tseng KY, O'Donnell P (2004): Dopamine-glutamate interactions controlling prefrontal cortical pyramidal cell excitability involve multiple signaling mechanisms. J Neurosci 24: 5131–5139. [PubMed: 15175382]
50. Wang J, O'Donnell P (2001): D1 dopamine receptors potentiate NMDA-mediated excitability increase in layer V prefrontal cortical pyramidal neurons. Cereb Cortex 11: 452–462. [PubMed: 11313297]
51. Gulledge AT, Jaffe DB (2001): Multiple Effects of Dopamine on Layer V Pyramidal Cell Excitability in Rat Prefrontal Cortex. J Neurophysiol 86: 586–595. [PubMed: 11495934]

52. Chen L, Bohanick JD, Nishihara M, Seamans JK, Yang CR (2007): Dopamine D1/5 Receptor-Mediated Long-Term Potentiation of Intrinsic Excitability in Rat Prefrontal Cortical Neurons: Ca^{2+} -Dependent Intracellular Signaling. J Neurophysiol 97: 2448–2464. [PubMed: 17229830]
53. Kwon H-B, Sabatini BL (2011): Glutamate induces de novo growth of functional spines in developing cortex. Nature 474: 100–104. [PubMed: 21552280]
54. Kozorovitskiy Y, Saunders A, Johnson CA, Lowell BB, Sabatini BL (2012): Recurrent network activity drives striatal synaptogenesis. Nature 485: 646–650. [PubMed: 22660328]
55. Kozorovitskiy Y, Peixoto R, Wang W, Saunders A, Sabatini BL (2015): Neuromodulation of excitatory synaptogenesis in striatal development. Elife 4: e10111. [PubMed: 26551563]
56. Pologruto TA, Sabatini BL, Svoboda K (2003): ScanImage: Flexible software for operating laser scanning microscopes. Biomed Eng Online 2: 13. [PubMed: 12801419]
57. Coupé P, Munz M, Manjón JV., Ruthazer ES, Louis Collins D (2012): A CANDLE for a deeper in vivo insight. Med Image Anal 16: 849–864. [PubMed: 22341767]
58. Guo L, Xiong H, Kim J-I, Wu Y-W, Lalchandani RR, Cui Y, et al. (2015): Dynamic rewiring of neural circuits in the motor cortex in mouse models of Parkinson's disease. Nat Neurosci 18: 1299–1309. [PubMed: 26237365]
59. Tritsch NX, Sabatini BL (2012): Dopaminergic Modulation of Synaptic Transmission in Cortex and Striatum. Neuron 76: 33–50. [PubMed: 23040805]
60. Santana N, Mengod G, Artigas F (2009): Quantitative analysis of the expression of dopamine D1 and D2 receptors in pyramidal and GABAergic neurons of the rat prefrontal cortex. Cereb Cortex 19: 849–860. [PubMed: 18689859]
61. Waddington JL (1986): Behavioural correlates of the action of selective D-1 dopamine receptor antagonists. Impact of SCH 23390 and SKF 83566, and functionally interactive D-1: D-2 receptor systems. Biochem Pharmacol 35: 3661–3667. [PubMed: 3535801]
62. Chourbaji S, Zacher C, Sanchis-Segura C, Dormann C, Vollmayr B, Gass P (2005): Learned helplessness: Validity and reliability of depressive-like states in mice. Brain Res Protoc 16: 70–78.
63. Radley JJ, Rocher AB, Miller M, Janssen WGM, Liston C, Hof PR, et al. (2006): Repeated stress induces dendritic spine loss in the rat medial prefrontal cortex. Cereb Cortex 16: 313–320. [PubMed: 15901656]
64. Radley JJ, Rocher AB, Rodriguez A, Ehlenberger DB, Dammann M, Mcewen BS, et al. (2008): Repeated stress alters dendritic spine morphology in the rat medial prefrontal cortex. J Comp Neurol 507: 1141–1150. [PubMed: 18157834]
65. Fasano C, Bourque MJ, Lapointe G, Leo D, Thibault D, Haber M, et al. (2013): Dopamine facilitates dendritic spine formation by cultured striatal medium spiny neurons through both D1 and D2 dopamine receptors. Neuropharmacology 67: 432–443. [PubMed: 23231809]
66. Saunders A, Macosko EZ, Wysoker A, Goldman M, Krienen FM, de Rivera H, et al. (2018): Molecular Diversity and Specializations among the Cells of the Adult Mouse Brain. Cell 174: 1015–1030.e16. [PubMed: 30096299]
67. Woolfrey KM, Srivastava DP (2016): Control of Dendritic Spine Morphological and Functional Plasticity by Small GTPases. Neural Plasticity, vol. 2016. Hindawi Limited. 10.1155/2016/3025948
68. Stachniak TJ, Ghosh A, Sternson SM (2014): Chemogenetic Synaptic Silencing of Neural Circuits Localizes a Hypothalamu→Midbrain Pathway for Feeding Behavior. Neuron 82: 797–808. [PubMed: 24768300]
69. Mahler SV, Vazey EM, Beckley JT, Keistler CR, McGlinchey EM, Kaufling J, et al. (2014): Designer receptors show role for ventral pallidum input to ventral tegmental area in cocaine seeking. Nat Neurosci 17: 577–585. [PubMed: 24584054]
70. Roth BL (2016): DREADDs for Neuroscientists. Neuron 89: 683–94. [PubMed: 26889809]
71. Shen W, Flajolet M, Greengard P, Surmeier DJ (2008): Dichotomous Dopaminergic Control of Striatal Synaptic Plasticity. Science 321: 848–851. [PubMed: 18687967]
72. Hare BD, Shinohara R, Liu RJ, Pothula S, DiLeone RJ, Duman RS (2019): Optogenetic stimulation of medial prefrontal cortex Drd1 neurons produces rapid and long-lasting antidepressant effects. Nat Commun 10: 223. [PubMed: 30644390]

73. Feder A, Parides MK, Murrough JW, Perez AM, Morgan JE, Saxena S, et al. (2014): Efficacy of Intravenous Ketamine for Treatment of Chronic Posttraumatic Stress Disorder. JAMA Psychiatry 71: 681. [PubMed: 24740528]
74. Peltoniemi MA, Hagelberg NM, Olkkola KT, Saari TI (2016): Ketamine: A Review of Clinical Pharmacokinetics and Pharmacodynamics in Anesthesia and Pain Therapy. Clin Pharmacokinet 55: 1059–1077. [PubMed: 27028535]
75. Veilleux-Lemieux D, Castel A, Carrier D, Beaudry F, Vachon P (2013): Pharmacokinetics of ketamine and xylazine in young and old Sprague-Dawley rats. J Am Assoc Lab Anim Sci 52: 567–70. [PubMed: 24041212]
76. Wahlstrom D, Collins P, White T, Luciana M (2010, 2): Developmental changes in dopamine neurotransmission in adolescence: Behavioral implications and issues in assessment. Brain and Cognition, vol. 72. NIH Public Access, pp 146–159. [PubMed: 19944514]
77. Freitas C, Perez J, Knobel M, Tormos JM, Oberman L, Eldaief M, et al. (2011): Changes in Cortical Plasticity Across the Lifespan. Front Aging Neurosci 3: 1–8. [PubMed: 21442044]
78. Li SC, Lindenberger U, Bäckman L (2010, 4): Dopaminergic modulation of cognition across the life span. Neuroscience and Biobehavioral Reviews, vol. 34. pp 625–630. [PubMed: 20152855]
79. Spear LP (2000): The adolescent brain and age-related behavioral manifestations. Neurosci Biobehav Rev 24: 417–463. [PubMed: 10817843]
80. Kalsbeek A, Voorn P, Buijs RM, Pool CW, Uylings HBM (1988): Development of the dopaminergic innervation in the prefrontal cortex of the rat. J Comp Neurol 269: 58–72. [PubMed: 3361004]
81. MacDonald SWS, Karlsson S, Rieckmann A, Nyberg L, Backman L (2012): Aging-Related Increases in Behavioral Variability: Relations to Losses of Dopamine D1 Receptors. J Neurosci 32: 8186–8191. [PubMed: 22699899]
82. Rothmond DA, Weickert CS, Webster MJ (2012): Developmental changes in human dopamine neurotransmission: Cortical receptors and terminators. BMC Neurosci 13: 18. [PubMed: 22336227]
83. Bryant KA, Altinay M, Finnegan N, Cromer K, Dale RM (2019): Effects of Repeated Intravenous Ketamine in Treatment-Resistant Geriatric Depression. J Clin Psychopharmacol 39: 158–161. [PubMed: 30742589]
84. Konietzny A, Bär J, Mikhaylova M (2017, 5): Dendritic actin cytoskeleton: Structure, functions, and regulations. Frontiers in Cellular Neuroscience, vol. 11. Frontiers Media S.A. 10.3389/fncel.2017.00147
85. Bachmann VA, Riml A, Huber RG, Baillie GS, Liedl KR, Valovka T, Stefan E (2013): Reciprocal regulation of PKA and Rac signaling. Proc Natl Acad Sci U S A 110: 8531–8536. [PubMed: 23657011]
86. Nagai T, Nakamuta S, Kuroda K, Nakauchi S, Nishioka T, Takano T, et al. (2016): Phosphoproteomics of the Dopamine Pathway Enables Discovery of Rap1 Activation as a Reward Signal In Vivo. Neuron 89: 550–565. [PubMed: 26804993]

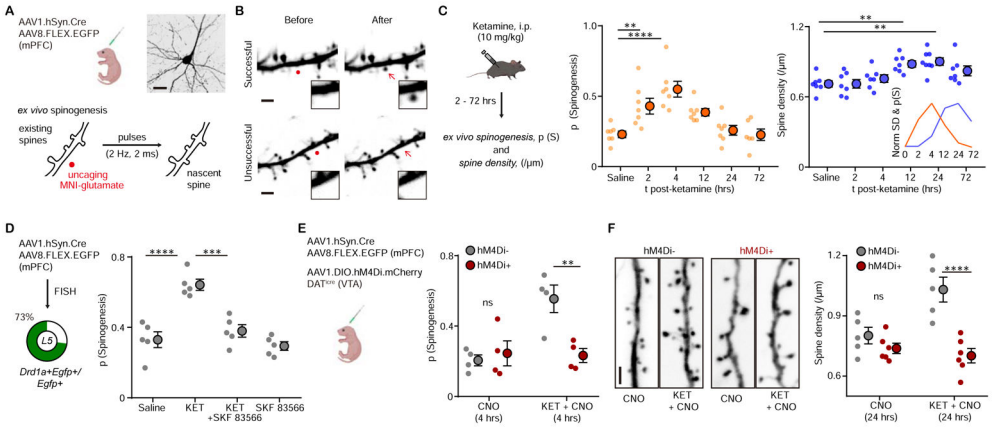

Figure 1. Ketamine regulates mPFC plasticity through a DA-dependent mechanism

(A). Schematic illustrating glutamate-evoked *de novo* spinogenesis platform. Top, viral transduction and an example EGFP^{+} pyramidal neuron in mPFC. Bottom, MNI-glutamate uncaging parameters for the induction of new dendritic spines. Scale bar, 50 μm.

(B). Example 2PLSM images of successful and unsuccessful induction trials of de novo spinogenesis. Red circles, uncaging sites. Black rectangle, close up images of local dendritic segments before and after glutamate uncaging. Scale bar, 2 μm.

(C). Left, schematic illustrating timecourse of ketamine treatments and experiments. Middle, timecourse of evoked spinogenesis probability on deep layer mPFC neurons in mice treated with either saline or ketamine (i.p. 10 mg/kg, acute slice preparation 2-72 hrs after treatment). Each small circle, aggregate probability of evoked spinogenesis from a single animal. Large circle, group data. n = 6 - 7 animals/time point, 15 - 25 trials/animal, one-way ANOVA, F (5, 35) = 9.895, $p < 0.0001$, Sidak's multiple comparison test vs Saline, 2 hrs $p = 0.076$, 4 hrs, $p < 0.0001$, 12 hrs, $p = 0.0532$, 24/72 hrs, $p > 0.9$. Right, same as left but for dendritic spine density. n = 7 - 8 animals/time point, one-way ANOVA, F (5, 37) = 6.319, $p = 0.0002$, Sidak's multiple comparison test vs Saline, 2/4 hrs $p > 0.8$, 12 hrs, $p = 0.0056$, 24 hrs, $p = 0.0011$, 72 hrs, $p = 0.1271$. Inset, normalized time course of changes in evoked spinogenesis (orange) and dendritic spine density (blue).

(D). Left, viral transduction and percentage of *Drd1a+Egfp+/Egfp+* cells in layer 5 mPFC. Right, probability of glutamate-evoked spinogenesis on deep layer mPFC neurons in mice treated with Saline, KET (10 mg/kg), KET + SKF 83566 (10 mg/kg), or SKF 83566 alone. Each small circle, aggregate probability of evoked spinogenesis from a single animal. Large circle, group data. One-way ANOVA, $p < 0.0001$, F (3, 16) = 20.29, Sidak's multiple comparison test, Saline vs KET, $p < 0.0001$, KET vs KET + SKF83566, $p = 0.0002$, Saline vs SKF83566, $p = 0.8574$.

(E). Left, schematic illustrating triple viral transduction strategy for evoked spinogenesis with DA neuron inhibition. Right, probability of spinogenesis on deep layer mPFC neurons in DAT^{iCre+} and DAT^{iCreG-} animals treated with CNO (3 mg/kg) across conditions (baseline, KET). n = 4 animals/condition as shown in plots, two-way ANOVA, Sidak's multiple comparison test, Cre− vs Cre+, CNO, $p = 0.8686$, CNO + KET, $p = 0.0042$.

(F). Left, example confocal images of EGFP expression in dendrites of deep layer mPFC pyramidal neurons, in response to CNO and ketamine treatment, as noted. Scale, 2 μm. Right, same as (E) but for dendritic spine density. n = 5 - 6 animals/condition as shown in

plots, two-way ANOVA, Sidak's multiple comparison test, Cre− vs Cre+, CNO, $p = 0.5005$, CNO + KET, $p < 0.0001$. Scale bar, 2 μm.

** $p < 0.01$, *** $p < 0.001$ **** $p < 0.0001$. Error bars reflect SEM.

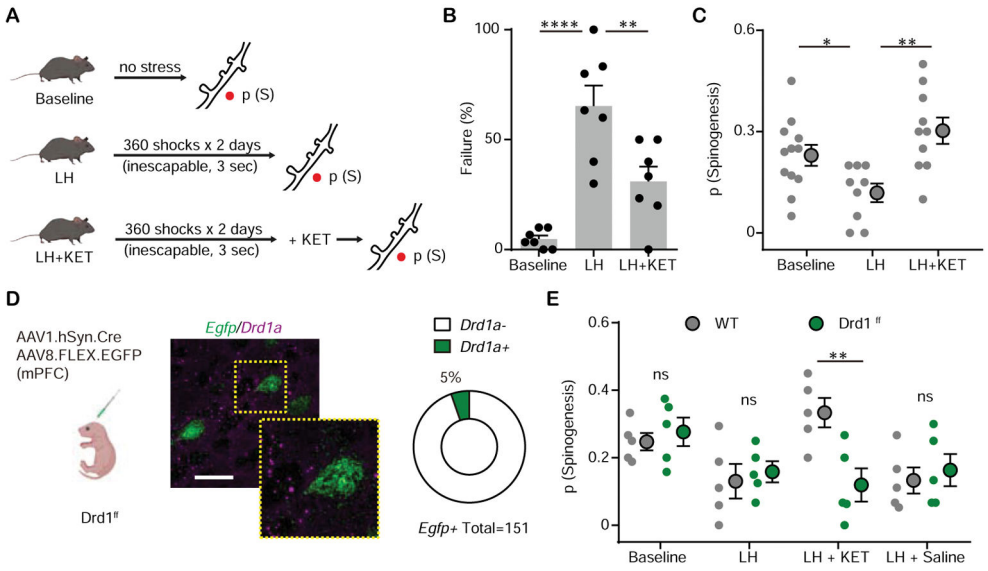

Figure 2. Ketamine rescues mPFC plasticity after stressful experience through Drd1 receptor

(A). Left, schematic illustrating glutamate-evoked spinogenesis assay in Baseline, LH, and LH + KET conditions.

(B). Summary data showing the percentage of failures to escape an escapable aversive shock, one-way ANOVA, $F(2, 18) = 20.26$, $p < 0.0001$, Sidak's multiple comparison test, Baseline vs LH, $p < 0.0001$, LH vs LH + KET, $p = 0.0041$.

(C). Probability of glutamate-evoked spinogenesis on deep layer mPFC neurons in distinct stages of aversive learning (baseline, LH, LH + KET). n = 9 - 12 animals/condition as shown in plots, one-way ANOVA, $F(2, 28) = 7.146$, $p = 0.0031$, Sidak's multiple comparison test, Baseline vs LH, $p = 0.0496$, LH vs LH + KET, $p = 0.0016$.

(D). Left, schematic illustrating dual viral transduction strategy with sparse genetic manipulation of Drd1 receptor expression in Drd1^{ff} mice. Middle, Fluorescence in situ hybridization (FISH) image confirming the absence of *Drd1a* mRNA expression (purple) in *Egfp* mRNA expressing mPFC cells (green) in Drd1^{ff} mice. Inset, close up of a single neuron. Scale bar, 50 μm. Right, quantification of the percentage of *Drd1a*+ cells among *Egfp*+ cells in mPFC. 5% *Drd1a*+ and 95% *Drd1a*– among 151 *Egfp*+ cells from 2 animals.

(E). Probability of glutamate-evoked spinogenesis on deep layer mPFC neurons in distinct stages of aversive learning (baseline, LH, LH + KET, LH + saline) in wild type and Drd1^{ff} mice. Two-way ANOVA, Sidak's multiple comparison test, WT vs Drd1^{ff}, LH + KET, $p = 0.0043$, Baseline, LH and LH + Saline, $p > 0.9$, n = 5 animals.

*$p < 0.05$, ** $p < 0.01$, *** $p < 0.001$ **** $p < 0.0001$. Error bars reflect SEM.

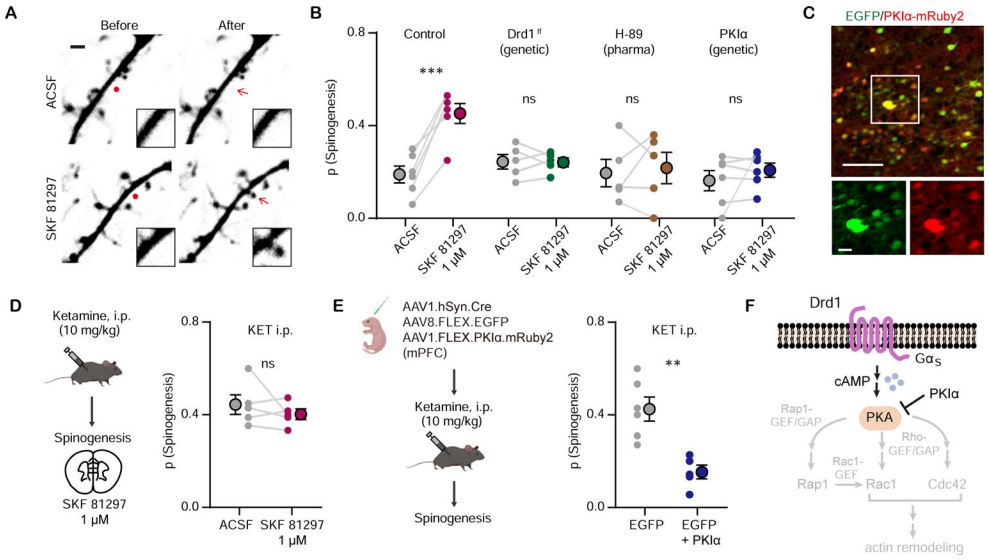

Figure 3. Drd1 activation promotes glutamate-induced spinogenesis in mPFC pyramidal neurons through PKA signaling

(A). Example 2PLSM images of *de novo* spinogenesis trials with ACSF or 1 μM SKF 81297. Red circles, uncaging sites. Black rectangle, close up images of local dendritic segments before and after glutamate uncaging. Scale bar, 2 μm.

(B). Probability of glutamate-evoked spinogenesis on deep layer mPFC neurons in brain slices with or without bath application of 1 μM SKF 81297. Slices were treated with 10 μM H-89 or collected from mice with genetic manipulation of GFP expressing pyramidal neurons (Drd1^{ff} or PKIα). Each small circle, aggregate probability of evoked spinogenesis from a single experiment. Large circles, group data. Paired two-tailed t test, ACSF vs SKF 81297, Control, p = 0.0007; Drd1^{ff}, p = 0.9249; H-89, p = 0.7351; PKIα, p = 0.4; n = 5 – 6 experiments/group.

(C). Top, colocalization of PKIα-mRuby2 in EGFP-expressing mPFC neurons. Bottom, close up images of EGFP and mRuby2 signals. Scale bar, 100 μm and 20 μm.

(D). Left, schematic illustrating glutamate-evoked spinogenesis assay in slices from mice pre-treated with ketamine (10 mg/kg, i.p.). Bottom, probability of glutamate-evoked spinogenesis on deep layer mPFC neurons in brain slices with or without bath application of 1 μM SKF 81297. Paired two-tailed t test, ACSF vs SKF 81297, p = 0.3745.

(E). Left, schematic illustrating triple viral transduction strategy for PKIα expression. Right, probability of glutamate-evoked spinogenesis in deep layer mPFC neurons in mice with or without PKIα expression, injected with ketamine (10 mg/kg, i.p.). Unpaired two-tailed t test, GFP vs GFP + PKIα, p = 0.0020.

(F). Schematic of simplified signaling pathways downstream of Drd1-PKA involved in actin remodeling in dendritic spines.

** p < 0.01, *** p < 0.001. Error bars reflect SEM.

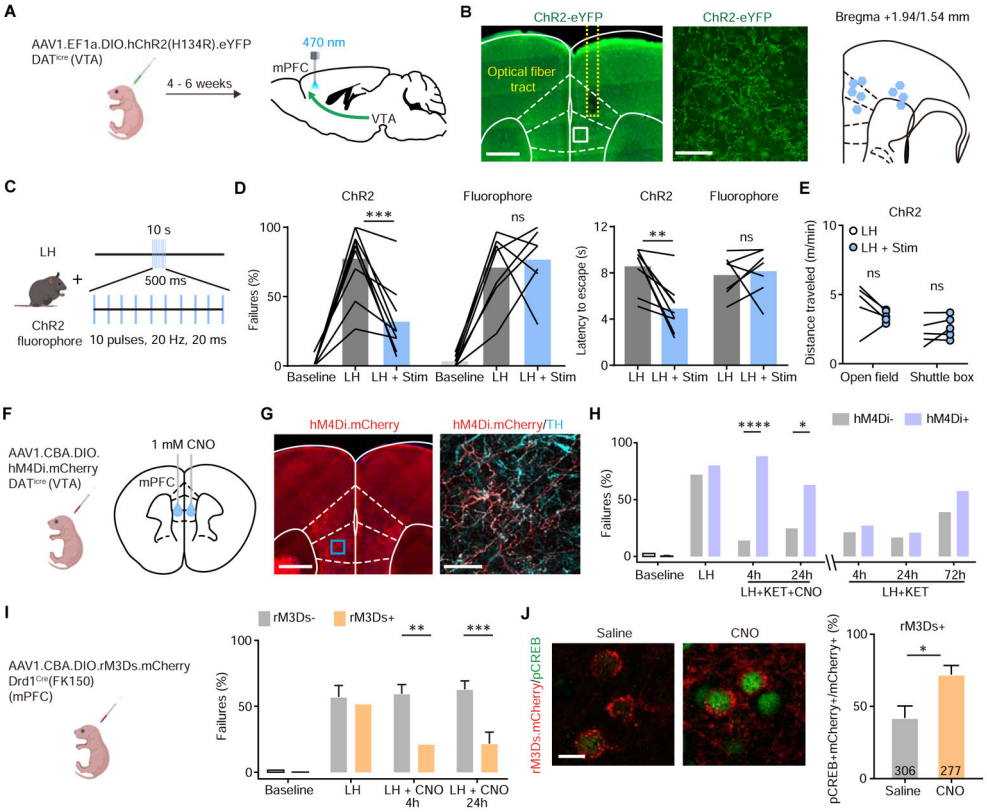

Figure 4. Activity of local DA terminals and Drd1+ neurons in mPFC mediates ketamine effects on behavior after stress

(A). Schematic for viral transduction with Cre-dependent ChR2 AAV in the VTA and subsequent optogenetic fiber implant in mPFC.

(B). Left, fiber placement illustration on a coronal section through mPFC, with a close up image of ChR2.eYFP terminals (white dashed lines, Paxinos atlas overlay; yellow dashed lines, fiber track). Green, immunoenhanced ChR2.eYFP; blue, Hoechst nucleic stain. Scale bars: 500 μm and 50 μm. Right, atlas location of fiber placement for each subject.

(C). Schematic illustrating open loop optogenetic stimulation parameters (Stim, optogenetic stimulation).

(D). Left, summary data showing the percentage of failures to escape an escapable aversive shock in ChR2-expressing mice (n = 9) and fluorophore-expressing controls (n = 7) across phases of learning, Baseline, LH, and LH + Stim. Right, summary data for latency to escape in LH compared with LH + Stim conditions. Repeated measures two-way ANOVA, Sidak's multiple comparison test, LH vs LH + Stim, ChR2, $p = 0.0002$, Fluorophore, $p = 0.9358$. Latency to escape, LH vs LH + Stim, ChR2, $p = 0.0014$, Fluorophore, $p = 0.9248$.

(E). Left, locomotion in the open field and shuttle box (m/min) after learning with and without optogenetic stimulation. Repeated measures two-way ANOVA, Sidak's multiple comparison test, open field, $p = 0.1742$, shuttle box, $p = 0.7503$, n = 5 mice.

(F). Left, schematic illustrating viral transduction strategy. Right, local CNO infusion in mPFC (1 mM, 1 μl).

(G). Left, immunoenhanced image of hM4Di.mCherry+ DAT+ terminals in mPFC. Right, mCherry+ terminals colocalize with a subset of tyrosine hydroxylase (TH) expressing axons. Scale bars, 500 μm and 50 μm.

(H). Summary data showing the percentage of failures to escape an escapable aversive shock across learning and treatment conditions for hM4Di-expressing DAT^{iCre} positive and negative littermates. n = 5 animals for Cre−, 8 animals for Cre+, two-way ANOVA, Sidak's multiple comparison test. KET + CNO 4 hrs, $p < 0.0001$, KET + CNO 24 hrs, $p = 0.0476$, KET + only 4, 24, and 72 hrs, $p > 0.7$.

(I). Left, schematic illustrating viral transduction strategy. Right, Summary data showing the percentage of failures to escape an escapable aversive shock in Drd1-Cre+ and Drd1-Cre− mice expressing rM3Ds across phases of learning and after CNO treatment (Baseline, LH, LH + CNO 4 hrs, and LH + CNO 24 hrs). n = 8 - 10 animals/condition, two-way ANOVA, Sidak's multiple comparison test, Cre+ vs Cre−, LH + CNO 4 hrs, $p = 0.0018$, LH + CNO 24 hrs, $p = 0.0007$, Baseline/LH, $p > 0.9$.

(J). Left, colocalization of pCREB immunolabeling and rM3Ds.mCherry expression in mPFC after Saline/CNO treatment in Drd1 Cre+ mice. Right, the quantification of percentage of pCREB+ cells among mCherry+ cells. Scale bar, 20 μm. n = 3 animals/condition cell number as noted in each bar, two-tailed unpaired t-test, $p = 0.0455$.

*$p < 0.05$, ** $p < 0.01$, *** $p < 0.001$, **** $p < 0.0001$. Error bars reflect SEM.

KEY RESOURCES TABLE

Resource Type	Specific Reagent or Resource	Source or Reference	Identifiers	Additional Information
Add additional rows as needed for each resource type	Include species and sex when applicable.	Include name of manufacturer, company, repository, individual, or research lab. Include PMID or DOI for references; use “this paper” if new.	Include catalog numbers, stock numbers, database IDs or accession numbers, and/or RRIDs. RRIDs are highly encouraged; search for RRIDs at https://scicrunch.org/resources.	Include any additional information or notes if necessary.
Antibody	Mouse anti-tyrosine hydroxylase	Abcam	Cat#AB129991; RRID: AB_11156128	
Antibody	Chicken anti-GFP	Abcam	Cat#AB13970; RRID: AB_300798	
Antibody	Rabbit anti-RFP	Rockland	Cat#600-401-379; RRID:AB_2209751	
Antibody	Rabbit anti-pCREB S133	Abcam	Cat#AB32096; RRID:AB_731734	
Antibody	Goat anti-rabbit Alexa 488/647	Thermo Fisher Scientific	Cat#A-11034/21244; RRID: AB_2576217, RRID: AB_2535812	
Antibody	Goat anti-chicken Alexa 488	Thermo Fisher Scientific	Cat# A-11039; RRID:AB_2534096	
Antibody	Goat anti-mouse Alexa 594	Thermo Fisher Scientific	Cat# A-11032; RRID:AB_2534091	
Bacterial or Viral Strain	AAV1.CBA.DIO.hM4Di.mCherry	Hou XH, 2016 Packaged by Vigene (Plasmid, Dr. Sabatini)	Addgene plasmid # 81008	
Bacterial or Viral Strain	AAV8.CAG.Flex.EGFP	UNC Vector Core (Dr. Boyden)	N/A	
Bacterial or Viral Strain	AAV1.hSyn.Cre.WPRE.Hgh	Penn vector core (Dr. Wilson)	ddgene viral prep # 105553-AAV1 Penn ID: AV-1-PV2676	
Bacterial or Viral Strain	AAV1.EF1a.DIO.hChR2(H134R).eYFP	Penn vector core (Dr. Deisseroth)	Addgene viral prep # 20298-AAV1, RRID:Addgene_20298	
Bacterial or Viral Strain	AAV1.CBA.DIO.rM3Ds.mCherry.WPRE	Packaged by Vigene (Plasmid, Dr. Roth)	Addgene plasmid # 50458 Custom cloning	
Bacterial or Viral Strain	AAV1.FLEX.PKI.IRES.nls.mRuby2	Chen et al, 2014 Packaged by Vigene (Plasmid, Dr. Sabatini)	Addgene plasmid # 63059	
Chemical Compound or Drug	Ketamine	Vedco	217-484-6; CAS: 1867-66-9	
Chemical Compound or Drug	Clozapine-N-oxide	Sigma-Aldrich	C0823; CAS: 34233-69-7	
Chemical Compound or Drug	SKF-83566 hydrobromide	Tocris	1586; CAS: 108179-91-5	
Chemical Compound or Drug	MNI-caged-L-glutamate	Tocris	1490; CAS: 295325-62-1	
Chemical Compound or Drug	SKF 81297 hydrobromide	Tocris	1447; CAS 67287-39-2	
Chemical Compound or Drug	H-89 dihydrochloride	Tocris	2910; CAS 130964-;39-5	
Commercial Assay Or Kit	RNAscope Fluorescence Multiplex Assay	ACDBio	Cat No. 320850	

Resource Type	Specific Reagent or Resource	Source or Reference	Identifiers	Additional Information
Commercial Assay Or Kit	RNAscope Probe- Mm-drd1a	ACDBio	Cat No. 406491-C2	
Commercial Assay Or Kit	RNAscope Probe- egfp	ACDBio	Cat No. 409971	
Deposited Data; Public Database	Raw and analyzed data	This paper		
Organism/Strain	Mouse: C57BL/6	Charles River	Cat#000664; RRID: IMSR_JAX:000664	
Organism/Strain	Mouse: B6.SJL-S1c6a3tm1.1(cre)Bkmn/J	Jackson Laboratory	Cat#006660; RRID: IMSR_JAX:006660	
Organism/Strain	Mouse: B6.FVB(Cg)-Tg(Drd1a-cre)FK150Gsat/Mmucd	Jackson Laboratory	RRID:MMRRC_036916-UCD	
Organism/Strain	Mouse: STOCK Drd1tm2.1St1/J	Jackson Laboratory	Cat#025700; RRID: IMSR_JAX:025700	
Recombinant DNA	pAAV-hSyn-DIO-rM3D(Gs)-mCherry	Addgene	Cat#50458	
Recombinant DNA	pAAV-CBA-DIO-WPRE-hGH Backbone	Addgene	Cat#81008	
Software; Algorithm	GraphPad Prism 7	GraphPad	RRID: SCR_002798	
Software; Algorithm	FIJI	Schindelin et al., 2012	http://fiji.sc/; RRID: SCR_002285	
Software; Algorithm	MATLAB	MathWorks	RRID: SCR_001622	
Software; Algorithm	Igor Pro	WaveMetrics	RRID: SCR_000325	
Software; Algorithm	Toxtrac	Rodriguez, A., et al., 2018	N/A	
Software; Algorithm	Python	Python Software Foundation	RRID:SCR_008394	
Software; Algorithm	CANDLE	The McConnell Brain Imaging Centre Coupé, P., et al., 2012	N/A	
Software; Algorithm	Neurolucida 360	MBF Bioscience	RRID:SCR_016788	
Other	Active/Passive Avoidance Shuttle Box	MazeEngineers	https://mazeengineers.com/portfolio/active-passive-avoidance-shuttle-box/#description	
Other	Raspberry Pi	Raspberry Pi Foundation	https://www.raspberrypi.org/	